Unraveling the Speciation of β-Amyloid Peptides during the Aggregation Process by Taylor Dispersion Analysis

Mihai Deleanu, Jean-François Hernandez, Luca Cipelletti, Jean Philippe Biron, Émilie Rossi, Myriam Taverna, Herve Cottet, Joseph Chamieh

▶ To cite this version:

Mihai Deleanu, Jean-François Hernandez, Luca Cipelletti, Jean Philippe Biron, Émilie Rossi, et al.. Unraveling the Speciation of β-Amyloid Peptides during the Aggregation Process by Taylor Dispersion Analysis. Analytical Chemistry, 2021, 93 (16), pp.6523-6533. 10.1021/acs.analchem.1c00527 . hal-03359470

HAL Id: hal-03359470
https://hal.science/hal-03359470

Submitted on 30 Sep 2021

Unraveling the speciation of β-amyloid peptides during the aggregation process by Taylor dispersion analysis

*Mihai Deleanu[1], Jean-François Hernandez[1], Luca Cipelletti[2,3], Jean-Philippe Biron[1], Emilie Rossi[4], Myriam Taverna[4], Hervé Cottet[*1], Joseph Chamieh[*1]*

[1]IBMM, Université Montpellier, CNRS, ENSCM, 34095 Montpellier, France

[2]Laboratoire Charles Coulomb (L2C), Université Montpellier, CNRS, Montpellier, France.

[3]Institut Universitaire de France (IUF), France

[2]Université Paris-Saclay, CNRS, Institut Galien Paris-Saclay, 92296, Châtenay-Malabry, France

[*] CORRESPONDING AUTHOR

Tel: +33 4 6714 3920, Fax: +33 4 6763 1046. E-mail: joseph.chamieh@umontpellier.fr

Tel: +33 4 6714 3427, Fax: +33 4 6763 1046. E-mail: herve.cottet@umontpellier.fr

ABSTRACT

The aggregation mechanisms of amyloid β peptides depend on multiple intrinsic and extrinsic physico-chemical factors (*e.g.* peptide chain length, truncations, peptide concentration, pH, ionic strength, temperature, metal concentrations…). Due to this high number of parameters, the formation of the oligomers and their propensity to aggregate make the elucidation of this physiopathological mechanism a challenging task. From the analytical point of view, up to our knowledge, few techniques are able to quantify, in real time, the proportion and the size of the different soluble species during the aggregation process. This work aims at demonstrating the interest of modern Taylor dispersion analysis (TDA) performed in capillaries (50 µm i.d.) to unravel the speciation of β-amyloid peptides in low volume peptide samples (~100 µL) with an analysis time of ~ 3 min per run. TDA was applied to study the aggregation process of Aβ(1-40) and Aβ(1-42) peptides at physiological pH and temperature, where more than 140 data points were generated with a total volume of ~1 µL over the whole aggregation study (about 0.5 µg of peptide). TDA was able the give a complete and quantitative picture of the Aβ speciation during the aggregation process, including the sizing of the oligomers and protofibrils, the consumption of the monomer, and the quantification of different early and late-formed aggregated species.

KEYWORDS. Taylor dispersion analysis; peptide aggregation; oligomers; amyloid beta peptides; diffusion coefficient; hydrodynamic radius.

Introduction

Alzheimer's disease (AD) is the result of a slow degeneration of neurons. It starts in the hippocampus (which lies in the medial temporal lobes of the brain and is responsible for the long-term memory) then extends to the rest of the brain. This fatal neurodegenerative disorder is characterized by progressive cognitive and functional impairment and memory loss[1]. Up till today, there is no cure for AD, however, there is extensive research to reveal its risk factors and the mechanisms leading to this dementia. Indeed, more than 95000 articles including more than 19000 reviews dealing with Alzheimer's disease were published just in the last decade (number of articles obtained on PubMed between 2010 and 2020 by searching "Alzheimer's disease").

For many years, AD was thought to be mainly associated to the formation of extracellular senile plaques composed primarily of amyloid β peptides (Aβ) and hyperphosphorylated neurofibrillary tangles of tau protein[2]. Consequently, research toward AD curative treatments has been driven largely by the amyloid cascade hypothesis. This hypothesis developed in the 1990's, relies on the fact that the most hydrophobic Aβ peptides (Aβ1-40 and mainly Aβ1-42) released by APP (Amyloid-β Precursor Protein) enzymatic cleavage, readily self-assemble to form amyloid species with evolving morphology and size (oligomers of increasing size, protofibrils and then fibrils) through a highly complicated process, finally accumulating into plaques which were believed to be the major pathogenic forms of Aβ[3,4]. More recently, production of soluble amyloid-β oligomers[5] and inflammation[6] have also emerged as important early steps in the pathogenesis of Alzheimer's disease. The "amyloid-β oligomer hypothesis" , which is still under debate, states that the main reasons behind AD is the formation of soluble oligomers of Aβ [7-10] considered to be more toxic than plaques and causing selective nerve cell death[10-12]. Indeed, soluble Aβ oligomers (AβO) are believed to be more toxic[13] than fibrils, which precipitate as plaques, because they are able to spread across neuronal tissue and they are supposed to mediate neurotoxicity and synaptic loss through binding to membrane receptors, including the prion protein[14,15]. To assess its validity and to develop new drug candidates against AD targeting the soluble oligomers, new analytical methodologies able to finely monitor, quantify and characterize these oligomeric species are required. However, in contrast to fibrils, which have low solubility and are highly stable, the soluble oligomers are fragile, metastable, transient[16], highly polydisperse in size, and therefore more difficult to detect and study in real time[16].

When studied *in vitro*, the aggregation mechanisms leading to the oligomers and then to fibrils depend on multiple physico-chemical factors, that can be intrinsic[17] (*e.g.* chain length, truncations, net charge, hydrophobicity) and extrinsic, such as concentration[18,19], pH, temperature, incubation conditions[20], buffer ionic strength and salt composition[21]. The influence of metals and other proteins has also been reported.[10] Due to this high number of parameters the elucidation of the aggregation mechanism is a challenging task. The detection of fibrils during the early stages of the aggregation process can be realized by multiple analytical techniques, and specifically by fluorescence using the ThT assay[22]. However, the ThT assay is mainly insensitive to Aβ oligomeric species[23]. In contrast, other analytical techniques are able to detect the presence of oligomers such as size exclusion chromatography (SEC)[24,25], AFM microscopy[26,27], capillary electrophoresis[28], mass spectrometry[29-31], and dynamic light scattering (DLS)[32], to name a few. However, some of the aforementioned methods require large sample volume (*e.g.* SEC), others are very sensitive to the presence of the large fibrils (or particles) making the detection of the small oligomers a difficult task (*e.g.* DLS). Few of these methods are able to follow in real time the aggregation process in a medium representative of the *in vivo* conditions. Furthermore, some of these techniques require a sample pretreatment before the analysis[25], which may alter the form of the species present in the sample. Thus, new methods able to rapidly determine the size of aggregates in the range 1-100 nm are highly required to better understand the real-time mechanism of oligomer formation.

In this context, Taylor Dispersion Analysis[33-35] (TDA) appears as a very promising alternative analytical method. Indeed, TDA is an absolute method (no calibration needed) allowing for the determination of the molecular diffusion coefficient, D, and of the hydrodynamic radius, R_h, of a solute, including for mixtures, without any bias in size, the contribution of the small and the large solutes being proportional to their mass abundance in the mixture[36]. TDA is based on the dispersion of an injected band under a laminar Poiseuille flow. Its implementation in narrow bore capillaries (typically ~50 µm i.d.) presents several advantages[37-40] such as a low sample consumption, a short analysis time, a wide range of sizing (from angstrom to sub-micron) and a straightforward analysis without any sample pretreatment or filtration [41-43].

In this work, TDA was applied to study the aggregation process of two Aβ isoforms Aβ(1-40) and Aβ(1-42) at physiological pH (7.4) and temperature (37°C) by providing a direct determination of all possible forms of Aβ amyloid according to the incubation time. TDA was able to provide a complete picture of the Aβ speciation during the in-vitro aggregation process, including the consumption of the monomer and the formation of oligomers, protofibrils and fibrils.

Materials and methods

Materials

Synthesized Amyloid beta (1-40) (denoted Aβ(1-40) in this work) was prepared as described in the *Solid-phase synthesis of Aβ(1-40)* section in the supporting information (Figure SI.1 shows a scheme of the synthesis protocol, while Figure SI.2 shows the chromatographic and mass spectrometry analysis of the synthesized peptide). Commercial Amyloid beta 1-40 (batch number 1658309, >95%) (denoted cAβ(1-40) in this work) was purchased from Anaspec (USA). Amyloid beta (1-42) (Aβ(1-42), batch number 1071428, >95%) was purchased from Bachem (Bubendorf, Switzerland). Thioflavin T, sodium dihydrogen phosphate, tris(hydroxymethyl)aminomethane, hydrochloric acid fuming 37%, sodium chloride and sodium hydroxide were purchased from Sigma Aldrich (France). *Fmoc* protected amino acids, coupling reagents HATU (Hexafluorophosphate Azabenzotriazole Tetramethyl Uronium) and PyBOP (benzotriazol-1-yl-oxytripyrrolidinophosphonium hexafluorophosphate) were purchased from Iris Biotech (Germany). The ChemMatrix H-Val-O-Wang resin was purchased from PCAS Biomatrix (Canada). Dimethylformamide, acetic anhydride, piperidine, dichloromethane, methanol, acetonitrile, trifluoroacetic acid and diethyl ether were acquired from Carlo Erba (Italy), Sigma-Aldrich (Merck, Germany), Acros Organics (Thermo Fisher-Scientific, Germany) or Honeywell-Riedel de Haën (Fisher-Scientific, Illkirch, France), and were all of analytical grade. *N*,*N*-diisopropylethylamine, 1,1,1,3,3,3-hexafluoro-2-propanol, triisopropylsilane (TIS) and tetra-*n*-butylammonium bromide were purchased from Alfa Aesar (Thermo Fisher-Scientific, Germany) or Fluorochem (UK). The ultrapure water used for all buffers was prepared with a MilliQ system from Millipore (France).

Peptide pretreatment

Both Aβ(1-40) and Aβ(1-42) were first pretreated independently as described elsewhere[28,44]. Briefly, Aβ(1-40) and Aβ(1-42) were dissolved in a 0.10 % (m/v) and 0.16 % (m/v) NH_4OH aqueous solution respectively to reach a final peptide concentration of 2 mg/mL. The peptide solutions were then incubated at room temperature for 10 min, separated into several aliquots and freeze-dried. The aliquot volume was calculated in order to obtain 10 nmol of peptide in each Eppendorf tube. The lyophilized peptide aliquots were stored at -20 °C until further use.

ThT fluorescence assay

In order to check the initial state of aggregation of the studied peptides, ThT fluorescence assay was used by adapting the protocol described in[45]. Briefly, peptides were dissolved at a concentration of 1 mM in a 1% NH_4OH aqueous solution, then diluted with 10 mM Tris-HCl + 100 mM NaCl buffer (pH 7.4) to a final concentration of 0.2 mM. A volume of 10 µL of the latter peptide solution was withdrawn and put in a Costar® 96-well black polystyrene plate along with 189 µL of 40 µM ThT in the Tris-HCl saline buffer solution. The fluorescence was monitored at room temperature for 24 h using a Berthold TriStar LB 941 instrument (Germany) (excitation wavelength 430 nm and emission wavelength 485 nm). Control wells were prepared by replacing the 10 µL of peptide solution with 10 µL of a 0.2% NH_4OH aqueous solution prepared by diluting a 1% NH_4OH aqueous solution with 10 mM Tris-HCl + 100 mM NaCl buffer (pH 7.4). Five wells were prepared for each solution.

Peptide aggregation study by Taylor dispersion analysis

TDA was performed on an Agilent 7100 (Waldbronn, Germany) capillary electrophoresis system using bare fused silica capillaries (Polymicro technologies, USA) having 40 cm × 50 µm i.d. dimensions and a detection window at 31.5 cm. New capillaries were conditioned with the following flushes: 1 M NaOH for 30 min; ultrapure water for 30 min. Between each analysis, capillaries were rinsed with 20 mM phosphate buffer, pH 7.4 (2 min). Samples were injected hydrodynamically on the inlet end of the capillary (44 mbar, 3 s, injected volume is about 7 nL corresponding to 1% of the capillary volume to the detection point). Experiments were performed using a mobilization pressure of 100 mbar. The temperature of the capillary cartridge was set at 37° C. The vial carrousel was thermostated using an external circulating water bath from Bioblock (France). The solutes were monitored by UV absorbance at 191 nm. The mobile phase was a 20 mM phosphate buffer, pH 7.4 (viscosity at 37°C is 0.7×10^{-4} Pa.s)[28]. Peptide samples were dissolved in 100 µL of 20 mM phosphate buffer, pH 7.4, to reach a final concentration of 100 µM and were immediately transferred to a vial and incubated at 37°C in the capillary electrophoresis instrument's carrousel. The aggregation was conducted by injecting the sample ($V_{inj} \approx 7$ nL) every 7 min in the case of Aβ(1-42) and each 30 min in the case of Aβ(1-40). The total number of TDA runs for each sample was about 150, corresponding to a total sample volume of 1050 nL (1.05 µL). To avoid sample evaporation, the vial cap was changed three times a day. The taylorgrams were recorded with the Agilent Chemstation software then exported to Microsoft Excel for subsequent data processing.

Dynamic light scattering

Complementary Dynamic Light Scattering data were acquired using a standard setup by Brookhaven Instruments Co. (BI-900AT), equipped with a 150 mW laser with in-vacuo wavelength $\lambda = 535$ nm. Frozen, dehydrated samples were thawed at room temperature. At time $t_{ag} = 0$, a volume of 100 µL of 20 mM phosphate buffer, pH 7.4, filtered through a 0.22 µm Millipore filter was added to the thawed powder, setting the Aβ 42 concentration to 100 µM. The sample was injected in an NMR tube and placed in the setup immediately after mixing. Measurements were performed as a function of t_{ag} by alternating runs at scattering angles $\theta = 90°$ and $\theta = 45°$ (run duration: 240 s and 360 s, respectively). The sample was thermostated at 37.0 ± 0.1 °C

The CONTIN algorithm[46,47] embedded in the Brookhaven software was used to extract $P_I(D)$, the intensity-weighted distribution of the diffusion coefficients D of the scatterers, which was then converted to the mass-weighted distribution of hydrodynamic radii R_h, $P_M(R_h)$, using custom software. In performing the conversion, it was assumed that the peptides aggregate by forming cylindrical structures resulting from the stacking of dimer units (see the discussion section and Figure 6). This allowed us to calculate the mass and scattered intensity (to within an inessential multiplicative constant) of the aggregates, as a function of their hydrodynamic radius, obtained via the HYDROPRO software[48]. Knowledge of $M(R_h)$ and $I(R_h)$ allowed for re-expressing $P_I(D)$ as $P_M(R_h)$, using standard probability distribution transformation laws and the Stokes-Einstein relationship $R_h = k_bT/(6\pi\eta D)$, with k_b Boltzmann's constant, T = 310.15 K, and η = 0.7 mPa s the solvent viscosity.

Results and discussion

ThT assay and the initial state of the peptide samples

The aggregation of Aβ peptides is a highly complex process that is dependent on, and very sensitive to, the initial conditions of the peptides preparation. The initial presence of aggregates (or seeds of aggregates) can drastically influence the aggregation process. Therefore, the peptides were treated upon reception with an ammonium hydroxide solution before freeze drying and storage[28]. The aim of this step is to dissociate any aggregated peptide and to start the kinetic studies from the very early steps, with a non-aggregated sample. To confirm the success of this step, samples were submitted to the ThT fluorescence assay[49]. Figure SI.3 shows the fluorescence kinetic curves of the studied peptide batches: the synthesized Aβ(1-40), the commercial cAβ(1-40), Aβ(1-42) and a control run. Only the commercial cAβ(1-40) was found to be initially aggregated, despite the ammonium hydroxide treatment, since it showed an initial relatively high fluorescence signal and nearly no lag phase. In contrast, the synthesized Aβ(1-40) and the commercial Aβ(1-42) peptides were assumed to be free of aggregates since their initial fluorescence intensity was low and in the same order of magnitude as the control run. These results show the importance of using clean (non-aggregated) samples for kinetic studies.

Processing of the taylorgrams

Briefly, the band broadening resulting from Taylor dispersion is easily quantified via the temporal variance (σ^2) of the elution profile. For that, a fit of the experimental peak with a Gaussian function allows for the determination of σ^2 and the calculation of the molecular diffusion coefficient, D, and consequently the hydrodynamic radius, R_h. The reader may refer to the supporting information for the theoretical aspects, equations and more details on the data processing.

The peptides were incubated at 37°C in a 20 mM phosphate buffer at pH 7.4. The aggregation was followed for 72 h and 12.5 h for Aβ(1-40) and Aβ(1-42), respectively. Figure 1 shows the taylorgrams recorded at selected incubation times for Aβ(1-40) (Figure 1A) and Aβ(1-42) (Figure 1B) while all experimental taylorgrams, for all incubations times t_{ag}, are shown in Figures SI.4 and SI.5. Importantly, the elution profile evolved faster in the case of Aβ(1-42) as compared to Aβ(1-40), suggesting a faster aggregation kinetics for this peptide. A second observation is that, for both studied peptides, the main peak observed at an elution time $t_0 \approx 2$ min, which represents the Aβ monomer at $t_{ag} = 0$, tended to broaden and to decrease in intensity during the aggregation process. This indicates the appearance of larger species and the decrease in concentration of the soluble species in the sample. At the end of the aggregation experiment, only a small sharp peak was observed (with a size corresponding to a small molecule/ion of about 0.4 nm, smaller than the size of the peptide monomer ~1.8 nm), indicating the disappearance of the soluble peptides, probably transformed into insoluble and larger aggregates that were not entering in the capillary, leading to the decrease in the peak area. At intermediate incubation times (*e.g.* t_{ag} between 0.5 h and ~11 h for Aβ(1-42)) the left side of the elution profile displayed spikes (very sharp peaks appearing before the main elution peak at elution times between 0.9 and 1.7 min), demonstrating the presence of very large species that are out of the Taylor regime[50,51] and rather belong to the so-called convective regime. In addition to the convective regime[50], large aggregates such as Aβ fibrils can also generate spikes, as seen in capillary electrophoresis and/or hydrodynamic flow of bacterial aggregates[52].

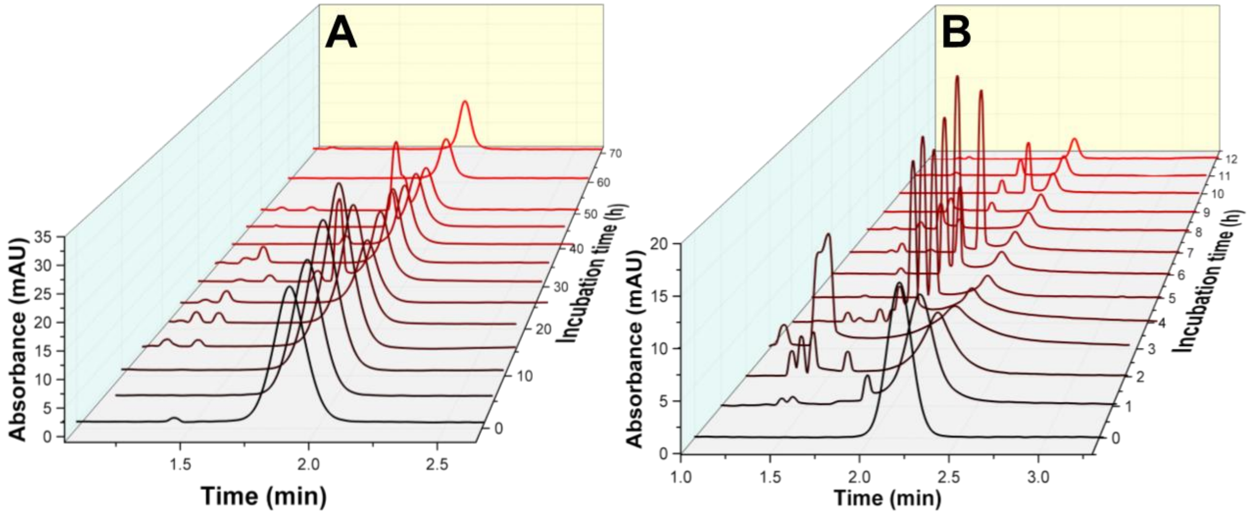

Figure 1. Three-dimensional overview of the obtained taylorgrams during the aggregation process of Aβ(1-40) (A) and Aβ(1-42) (B) at different incubation times. Experimental conditions: Sample: 100 µM; 20 mM phosphate buffer, pH 7.4. Incubation: quiescent conditions at 37 °C. Fused silica capillaries: 50 µm i.d. × 40 cm × 31.5 cm. Mobile phase: 20 mM phosphate buffer, pH 7.4. Mobilization pressure: 100 mbar. Injection: 44 mbar for 3 s, $V_i \approx 7$ nL ($V_i / V_d \approx 1$ %). Analyses were performed at 37 °C. UV detection at 191 nm.

In general, the obtained elution profiles were not Gaussian meaning that the sample was polydisperse in size. All taylorgrams were fitted on the basis of the right-side elution profile (*i.e.*

$t > t_0$, with t_0 the peak time) to get rid of the spikes that are present on the left side. The deconvolution of the right-side of the taylorgram provides valuable information on the aggregation process. Indeed, a complex mixture of components was obtained, composed of varying proportions of Aβ monomer, intermediate oligomers (R_h lower than 50 nm), protofibrils (R_h between 50 and 150 nm), small molecules (salts, counter ions…) and fibrils/insoluble aggregates (typical dimensions having an average diameter of approximately 7 – 10 nm and lengths up to several micrometers were reported for fibrils[53-55], they are detected as spikes on the taylorgrams). Except for the fibrils and other insoluble aggregates, all components in the mixture could be sized and quantified by TDA. For that, all the elution profiles were deconvoluted using two different approaches to extract the size and proportion of the different populations. A first fitting approach consisted in using a finite number of Gaussian curves ($n = 1 - 4$). The second fitting approach used the Constrained Regularized Linear Inversion (CRLI) algorithm, which does not require any hypothesis on the number of populations and allows obtaining a continuous distribution of the diffusion coefficient or of the hydrodynamic radius[56].

Figure SI.6 in the supporting information shows two typical examples of deconvolution of a TDA profile for Aβ(1-40) (Figure SI.6A) and Aβ(1-42) (Figure SI.6B), at selected incubation times t_{ag}= 25.52 h and t_{ag}= 1.98 h, respectively. In these examples, four Gaussian functions were used to fit the elution profile, with low residues for the curve fitting on the right side of the profile (see upper part of each Figure). When a lower number of Gaussian functions ($n \leq 3$) was used, the residues were much higher (see Figure SI.7). It is worth noting that a constraint was added to the fitting procedure on the value of the peak variance of the monomer population, allowing it to vary within 5 % with the respect to that at $t_{ag} = 0$ h (initial size of the monomers). Figures SI.8 and SI.9 show the Gaussian peaks extracted from the 4-Gaussian fit for the four populations and for both peptides, together with their respective area as a function of incubation time.

Monitoring Aβ(1-40) and Aβ(1-42) aggregation by TDA.

Figure 2 shows the monitoring of Aβ(1-40) (Figure 2A) or Aβ(1-42) (Figure 2B) aggregation using the aforementioned data processing. The lower panels of Figure 2 represent the evolution of the peak area of each population (proportional to its mass abundance), while the middle and upper panels represent the evolution in size (R_h) of these populations. The populations were classified by size into four groups. In the first group, some small molecules (R_h = 0.3 – 0.4 nm) were detected (blue down triangles). Their size as well as their abundance (peak area) were constant throughout the aggregation, and their presence seems therefore not related to the aggregation process. The second population (red squares) had a size of 1.99 ± 0.09 nm for Aβ(1-40) and 1.94 ± 0.12 nm for Aβ(1-42), and was attributed to the monomeric and small oligomeric forms of the peptides (up to dodecamers, see next section). The third population was attributed to higher molar mass oligomers with R_h between 4 and 50 nm. The average size of this population over the whole aggregation process was 24.9 ± 10.3 nm for Aβ(1-40) and 10.8 ± 6.1 nm for Aβ(1-42). The fourth population with R_h > 50 nm was attributed to soluble protofibrillar structures with an average size of 119 ± 49 nm for Aβ(1-40) and 110 ± 39 nm for Aβ(1-42).

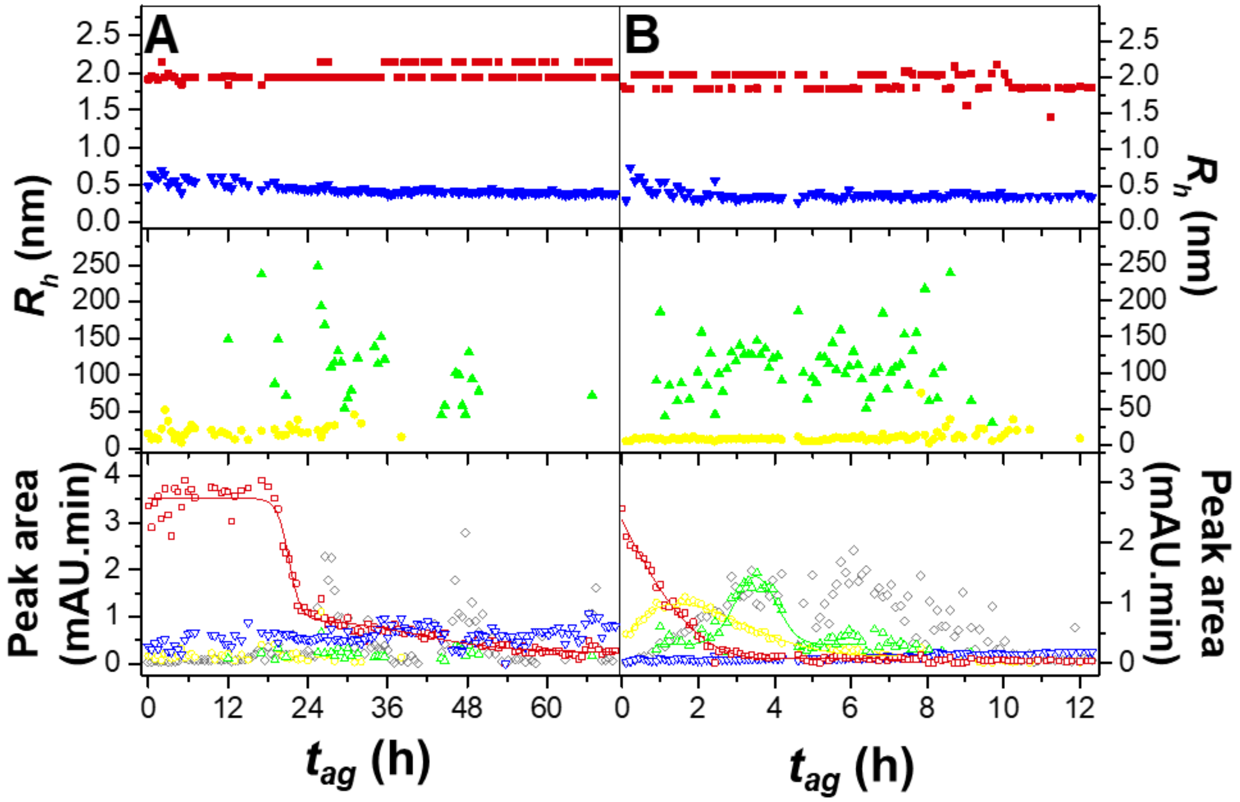

Figure 2. Hydrodynamic radius and peak area evolution of the different populations observed during the aggregation process of Aβ(1-40) (A) and Aβ(1-42) (B) using a 4 Gaussians fitting of the taylorgrams. Closed symbols are for the hydrodynamic radius: small molecules (B), monomer and low molar mass oligomers (!), higher molar mass oligomers (,), and soluble protofibrils (7). Open symbols correspond to the peak area of each species: small molecules (X), monomer and low molar mass oligomers (∀), higher molar mass oligomers (–), soluble protofibrils (8) and fibrils (M) (spikes). The straight lines are guides for the eyes. Experimental conditions as in Figure 1.

For the Aβ(1-40), only the monomeric and low molar mass oligomers populations were significantly present in the sample (see open red squares in Figure 2A), as compared to the high molar mass oligomers and protofibrils populations (open yellow circles and open green triangles, respectively), which were much less abundant. The red traces in Figure 2A showed that Aβ(1-40) was essentially in its monomeric form and remained so up to t_{ag} ~18 h. Afterwards, the peak area of the monomeric population rapidly dropped to reach a lower plateau at t_{ag} ~ 24 h. It is important to note that despite the disappearance of the monomeric form, no other soluble species yielded a significant signal in TDA. Indeed, the aggregation of Aβ(1-40) displayed a threshold-type behavior, which indicates that the rate-determining step for aggregation is the formation of multimeric seeds. In other words, our results seem to indicate that Aβ(1-40) goes through a secondary nucleation mechanism where monomers add to already present fibrils to elongate them and to produce larger fibrils, without going through intermediate species in accordance with what is discussed in the literature[57,58]. To confirm this hypothesis, a slight manual shaking of the vial was done at 25 h, 48 h and 70 h, in order to resuspend any precipitate/fibrils that may have sedimented. After each remixing, a significant increase of the peak area of the "spikes" (open grey diamonds in the lower part of Figure 2A) was transiently observed, proving the presence of insoluble species in the sample that suspend upon shaking and then tend to decant.

The aggregation process for Aβ(1-42) displayed a different pathway as compared to that of Aβ(1-40). For Aβ(1-42) the proportion of monomeric and low molar mass oligomeric populations decreased rapidly, while the higher molar mass oligomeric species increased to reach a maximum at t_{ag} = 1.6 h, after the disappearance of the monomeric species. Subsequently, the protofibrils proportion increased to reach a maximum at t_{ag} =3.5 h, and finally the spikes (non-diffusing species in suspension) increased to reach a maximum at t_{ag} = 5.6 h. From these observations, it is evident that TDA experiments gives a clear picture of the early stages of the aggregation process of the Aβ(1-42) that goes through a primary nucleation leading to intermediate species and successively an elongation step producing protofibrils and then fibrils.

The results for Aβ(1-40) and Aβ(1-42) obtained by fitting the taylorgram to *n* Gaussians were compared to the evolution of the R_h distributions obtained by CRLI[56], as shown in the supporting information (Figures SI.10, SI.11, SI.12 and SI.13). Continuous distributions of the hydrodynamic radius for each run (Figures SI.10 and SI.11) were obtained by CRLI algorithm, allowing for a full and quantitative characterization of the aggregation process. The CRLI analysis confirmed the two different pathways that were inferred for the aggregation of Aβ(1-40) and Aβ(1-42) on the basis of the *n*-Gaussians fits.

Another way to qualitatively and visually assess the entire aggregation process and the speciation of the amyloid peptides during the aggregation process is shown in Figure 3, which displays a stacked bar representation of the peak area of each population. The grey region represents the insoluble species that can enter the capillary and appear as spikes as well as those that precipitate and no longer enter in the capillary at the injection step, lowering the total observed peak area over incubation time. From this Figure, one can clearly distinguish the two different aggregation pathways[32,59].

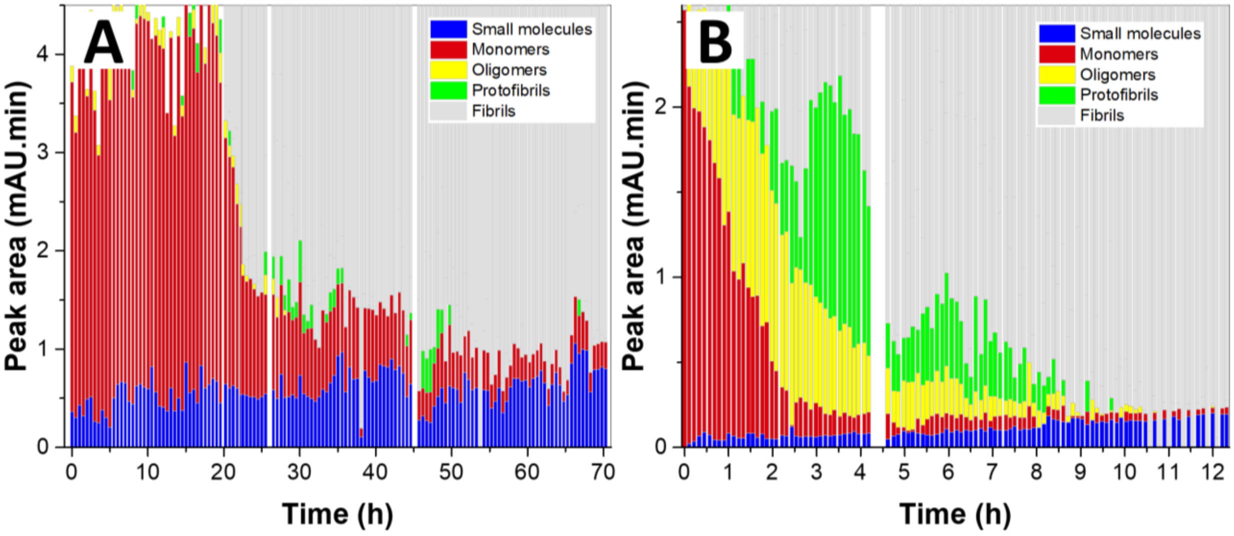

Figure 3. Stacked bar graphs showing the speciation of Aβ(1-40) (A) and Aβ(1-42) (B) at each analyzed incubation time obtained by TDA. Experimental conditions as in Figure 1. Four populations are distinguished: "small molecules" for R_h~0.4 nm; "monomers" for the monomer and the low molar mass oligomers with R_h~1.9 nm, "oligomers" for high molar mass oligomers with R_h between 4 and 50 nm; and "protofibrils" for large diffusing soluble species with R_h

between 50 and 150 nm. Each population is represented by the corresponding peak area obtained by 4 Gaussian curve fitting. The population in grey represents the fibrils but were not quantified by TDA and are just represented by difference.

To confirm these observations, the ThT assay was realized in the same conditions as the TDA analysis. The ThT assay is best known to detect the amyloid fibrillary structures, which are formed at the expense of the soluble ones causing a decrease in their proportion. As seen in Figure SI.14, the ThT assay curve superimpose on the concentration evolution of the insoluble species determined by TDA, demonstrating that TDA faithfully captures the lag phase and the time to reach the plateau of the aggregation process. Additionally, TDA allowed for a quantitative estimation of the intermediate steps of the aggregation , especially in the case of Aβ(1-42), a feature difficult to obtain[57] with other techniques such as SEC[25].

Discussion on the size of the Aβ species during the aggregation process.

Regarding the size of the aggregated forms, it was suggested from combined results obtained by NMR, FTIR and AFM, that Aβ(1-42) rapidly forms low molar mass oligomers upon solubilization[60]. The predominant forms ranged from dimer to dodecamer[59,61] including some assemblies (from tetramer to octamer) called “paranuclei”[32], which were in equilibrium with the lower molar mass oligomers. Several methods were used in the literature to identify the nature of these oligomers. Ion mobility MS allows to get structural information relative to the oligomeric molar mass distribution[29], however, the separation is obtained in gas phase which can perturb the oligomeric distribution. Further, ion suppression effect may also occur for quantitative analysis in complex mixtures[62]. Real-time aggregation monitoring methods such as dynamic light scattering (DLS) are very difficult to apply to detect the presence of small oligomers in polydisperse samples, especially in the presence of large aggregates. TDA has the advantage of being less sensitive to the presence of very large aggregates[36,63] allowing the detection of the early stage species, without bias in the mass-weighted size distribution. For the sake of comparison, DLS experiments were realized on the Aβ(1-42) sample in the same conditions as in TDA. From the obtained size distributions, $P_M(R_h)$, we integrated over four intervals, so as to obtain the mass-weighted relative contribution of four classes of aggregates, with $R_h < 5$ nm, 5 nm $< R_h <$ 50 nm, 50 nm $< R_h <$ 500 nm, and $R_h > 500$ nm, respectively (see Methods for details). Figure SI.15 shows the time evolution of the (mass-weighted) fractions of the four classes of aggregates thus obtained. The data shown in the figure correspond to the average of results obtained by processing separately data collected at scattering angles $\theta = 90°$ and $\theta = 45°$; x and y error bars indicate the half-difference between the corresponding pairs of data at 90° and 45°. In contrast to TDA results, dimers and small oligomers, corresponding to $R_h < 5$ nm, are not detected by DLS, because their scattered intensity is much weaker than that of larger species. On the other hand, DLS detects large aggregates, including objects up to several hundred nm, which are beyond the range accessible to TDA. Aggregates with $R_h > 500$ nm are detected as early as at $t_{ag} = 500$ s. Their relative contribution increases significantly for $t_{ag} > 1200$ s (0.33 h), at the expenses of both intermediate (50 nm $< R_h <$ 500 nm) and smaller (5 nm $< R_h <$ 50 nm) aggregates. These results show that DLS is a powerful technique able to follow in real time the evolution of the larger size species. However, in contrast to TDA, the sensitivity of DLS toward the smaller size species is quite limited. Thus, TDA and DLS are complementary methods.

In order to propose possible oligomeric structures that fit with the size of each population found by TDA, molecular simulation was performed based on Aβ(1-42) monomers (folded and unfolded)[64] and oligomers[65,66] structures found in the literature (low and high molar mass, from 2 to 360 monomer units). Different 3D molecular structures were constructed using the UCSF

Chimera X software[67] that were next loaded into HYDROPRO+[48] software to calculate the hydrodynamic properties. The 3D structures were adjusted so that the calculated translational diffusion coefficients equals the experimental values obtained by TDA for each population. Figures 4 and 6 display possible conformations for small and large oligomers thus obtained.

Different Aβ(1-42) monomer structures were considered, based on the structures published by Tomaselli *et al.*[64] (PDB code 1Z0Q), Lührs *et al.*[68] (PDB code 2BEG) and Colvin *et al.*[66] (PDB code 5KK3). Results show hydrodynamic radii around 1.5 nm for the different conformations (see Figure 4, monomer structures). The average hydrodynamic radii of the “monomer and small oligomers” population obtained by TDA on all runs over the whole Aβ(1-42) aggregation study (t_{ag} = 12.5 h, n = 110 TDA runs) was of 1.94 nm (RSD = 5.9 %) and the initial size at t_{ag} = 0 h was 1.84 nm. To correlate the observed experimental size with oligomeric structures, different proposed oligomeric structures from the literature, ranging from dimer to dodecamer with different conformations were used and computed to get the hydrodynamic radii (Figure 4) (PDB codes 5AEF[69], 2NAO[70], 5HOX[71], 6RHY[72] and 2MXU[73]). The latter structures were determined by electron cryo-microscopy[69], solid state NMR[70,73], X-ray crystallography[71] and NMR[72]. The combination of our results and those from the literature, suggest that the “monomer and small oligomers” population at t_{ag} = 0 h was mainly composed of monomers and dimers[74]. The weight-average R_h obtained by TDA is sensitive to the mass proportion of all the soluble species present in the mixture. The CRLI analysis brings additional information about the polydispersity of each population mode (see Figure 5). However, due to the low difference in R_h of the various small species (monomers / dimers / trimers) neither the CRLI nor the Gaussian fitting approaches were able to resolve these small species. CRLI shows that the size distribution of the “monomer and small oligomers” population at t_{ag} = 0 h ranges between 1 and 3 nm and is centered around 1.9

nm. The polydispersity in size of this mode increases with increasing incubation times. This population becomes negligible after t_{ag} ~ 2 - 4 h. Several reports[75-77] suggested the presence of a critical nucleus size, which is the minimum size that enables the extension of amyloid fibrils. To our knowledge, no consensus was reached on the exact size of the nuclei, while other reports stated that the nucleation was heterogeneous[78,79]. However, aggregation numbers between 2 and 14 were reported[75-77,80,81], which according to this work would correspond to a size distribution between 1.8 and ~3 nm, thus the first oligomer size population found by TDA.

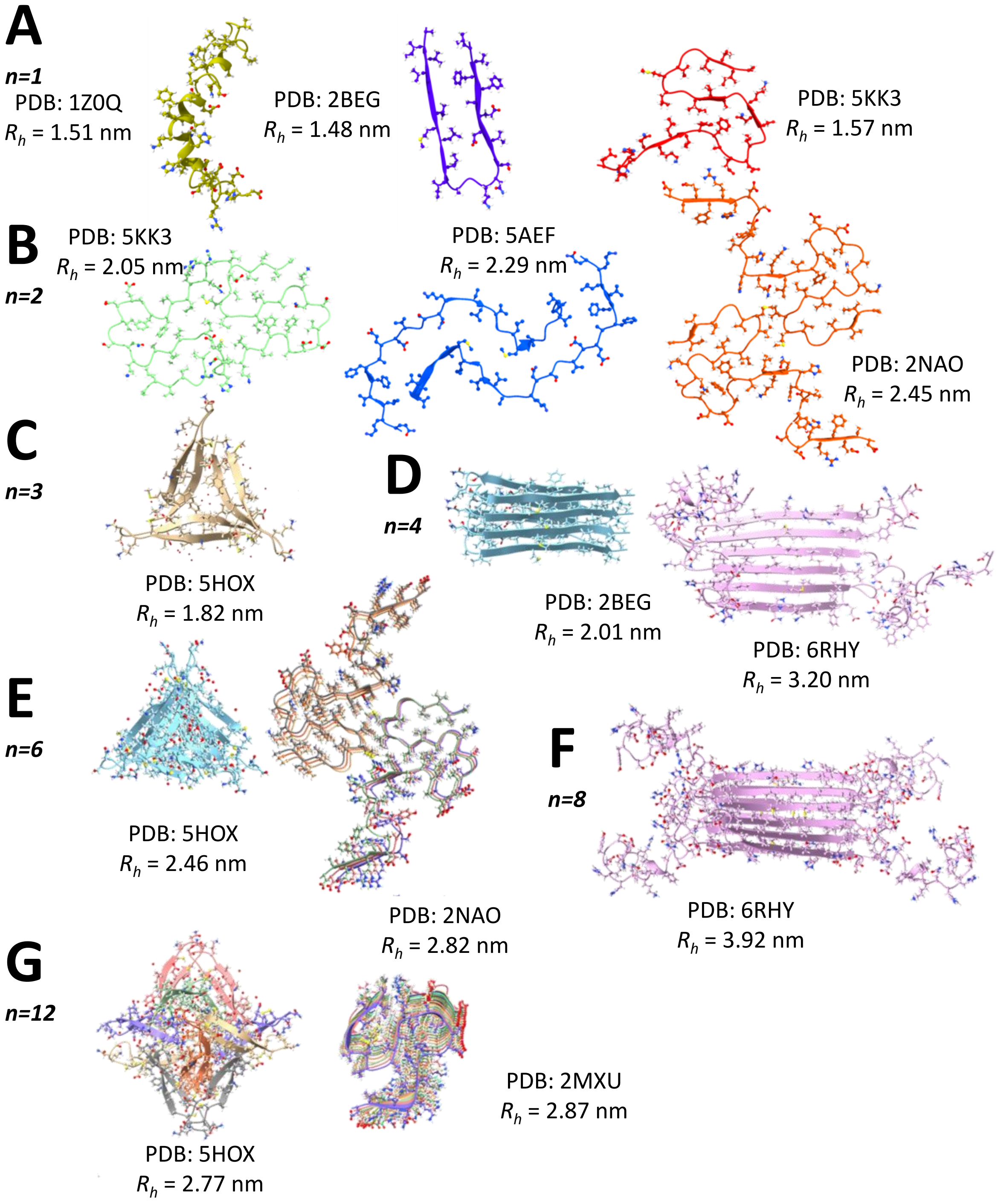

Figure 4. Schematic representation of the monomeric Aβ(1-42) (A) and small-oligomer conformations from dimers to dodecamers (B to G represent dimers, trimers, tetramers, hexamers, octamers and dodecamers respectively). The 3D structures were realized using the UCSF Chimera X software[67] and were adapted from the structure found in the literature (PDB codes 1Z0Q[64], 2BEG[68] and 5KK3[66]). The arrangement of the monomers in the oligomeric forms were adapted from the literature (PDB codes 5AEF[69], 2NAO[70], 5HOX[71], 6RHY[72] and 2MXU[73]).

The R_h were calculated by introducing the generated PDB files for each structure into the HYDROPRO software[48]. It is worth noting that the R_h calculation takes into account all possible orientations of the molecular structure relative to the flow direction.

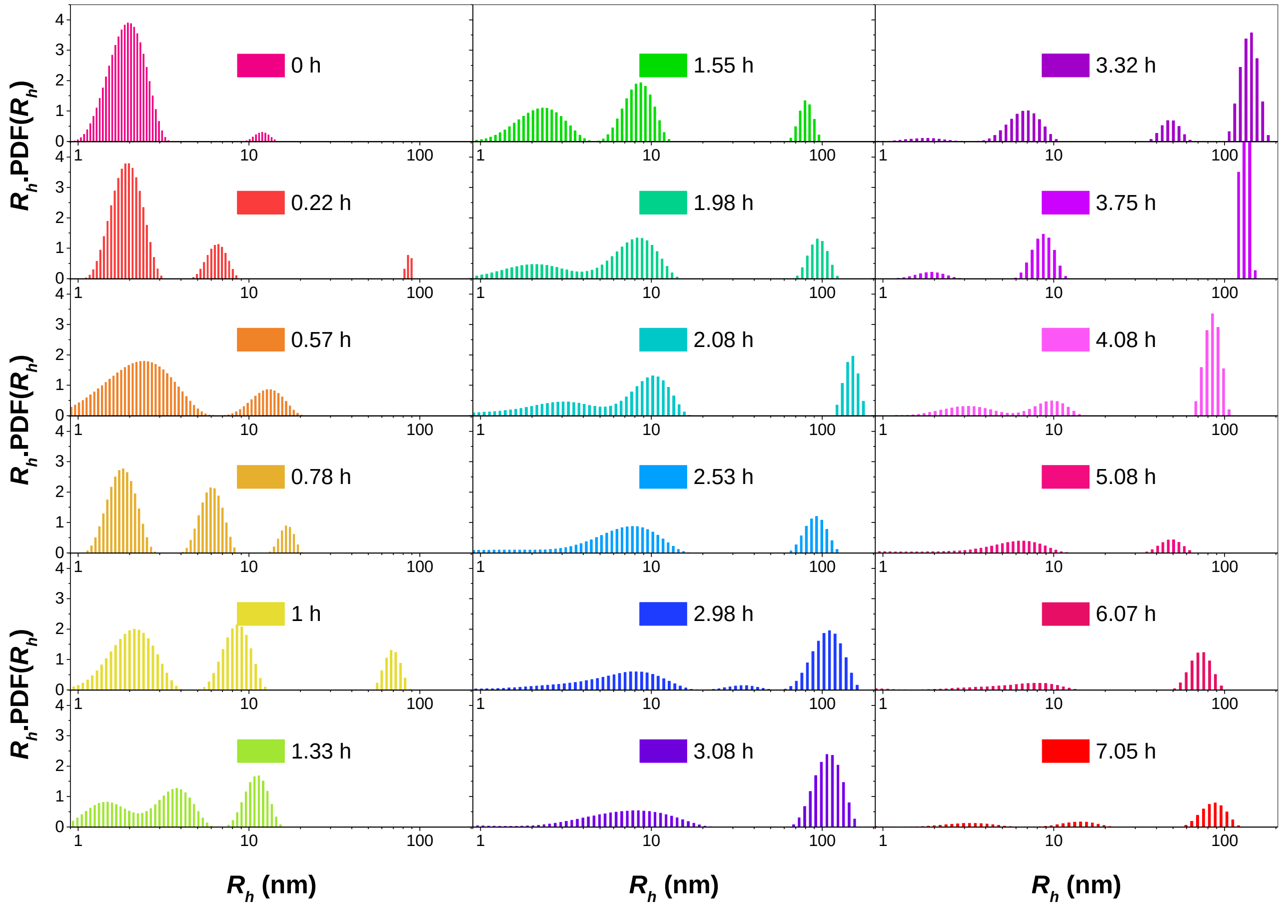

Figure 5. Size distributions of Aβ(1-42) obtained by CRLI analysis of the experimental taylorgrams as a function of incubation time t_{ag} = 0 to 7 h. Experimental taylorgrams and conditions as in Figure 1.

In order to identify the structure beneath the distribution of the “high molar mass oligomer” population, the same approach was applied by constructing 3D models and calculating their hydrodynamic radii. In fact, several NMR[66,70] or cryo-EM[82] studies have shown that the fibril core of Aβ(1-42) consisted of a dimer, each monomer containing four β-strands in an S-shaped amyloid fold arrangement (Figure SI.16). On these grounds, protofibrillar and fibrillar structures were constructed, using the PDB file code 5KK3[66], to get structures having a parallel superposition of dimers and ranging from one dimer unit (disc shaped with a width of ~6.4 nm and a length of ~0.9 nm) up to 720 dimer units (cylinder shaped with a width of ~6.4 nm and a length of ~345 nm). The calculated size for the constructed oligomers is given in Table SI.1 and in Figure 6. From the TDA analysis, the minimum size calculated for the high molar mass oligomers distribution based on the results obtained on the simulated structures in Figure 6 was 5.1 nm, and corresponded to an oligomer having 33 dimer units (~300 kDa) and dimensions of 17 nm in length and 3.2 nm in radius. The maximum size was 36 nm corresponding to approximately 700 dimer units (~6300 kDa) and dimensions of ~335 nm in length and 3.2 nm in radius. Further, over the whole aggregation process (110 TDA runs), the average size was 10.7 nm corresponding to a cylinder-shaped oligomer having ~115 dimer units (~1035 kDa) with a 57 nm length and a 3.2 nm radius. The CRLI analysis on the TDA runs of Aβ(1-42) aggregation (Figure 5) showed that the "high molar mass oligomer" population, centered around 10 nm, was present at t_{ag} = 0 h at a very low concentration as compared to that of the "monomer and small oligomers" population. These observations are in agreement with data obtained on Aβ(1-42) by FCS where stable micelle-like oligomers with a size of $R_h \approx 7 - 11$ nm and having 28 - 88 mers were observed[83]. The abundance of this population then increased with incubation time to reach a maximum at 2h, and finally became negligible after about 7 h.

Further, both the deconvolution using *n* Gaussian functions and the CRLI analysis showed that a larger sized population, appeared after 1h and reached a maximum at 3h, and then became negligible after 7h. We attributed this population to protofibrils since they are still soluble. Indeed, TDA has shown that this population had a size (R_h) ranging between 50 and 240 nm with an average value of 113 nm over the whole aggregation process (*n* = 110 TDA runs). If the same calculations were naively applied as done for the "high molar mass oligomers", structures having a length between 500 nm and up to 8.5 µm would be obtained, with an average length around 2.2 µm. The number of dimer units in these estimated elongated structures would range between 1200 and 18000 (average of 4650) (with a molar mass per unit length of about 19 kDa/nm). Nevertheless, one should keep in mind that TDA cannot give reliable information about the shape of these assemblies, only the R_h distribution is obtained. Other techniques such as AFM would be more suited for looking at the molecular structure[84,85]. Despite this limitation, which is common to all methods based on the determination of the diffusion coefficient (or R_h), the present work demonstrates that TDA in combination with molecular simulations can rapidly and advantageously propose a limited number of possible molecular conformations that are consistent with the experimental data.

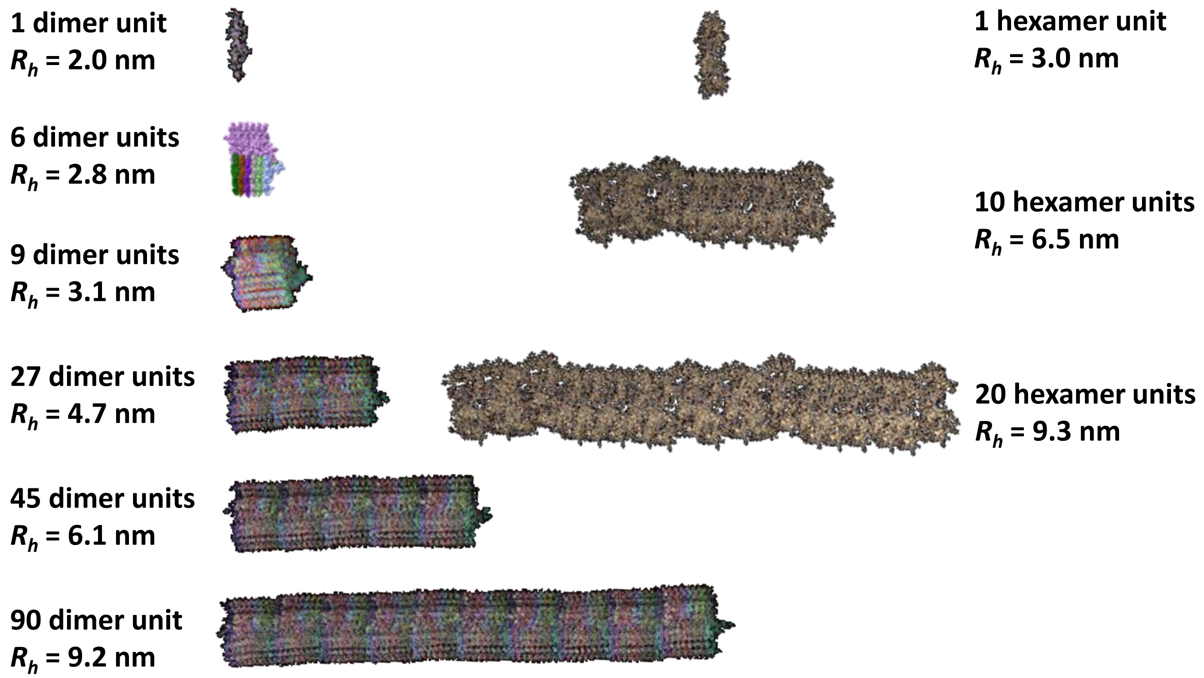

Figure 6. Schematic side view representation of possible conformations for the "high molar mass oligomeric Aβ(1-42)" population. The arrangement of the monomers in the oligomeric

form was based on the structures described by Colvin *et al.*[66] and in Tran *et al.*[65]. The 3D structures were realized using UCSF Chimera X software[67] and were adapted from the structure published in[64] (PDB code 1Z0Q) for the hexameric structures and in[66] (PDB code 5KK3) for the dimeric structures. The R_h were calculated by introducing the generated PDB files for each structure into HYDROPRO software[48]. The dimer, the hexamer, the dodecamer and the octadecamer, which size is lower than 4 nm, are represented for the sake of comparison.

Finally, reports from the literature found that toxic Aβ oligomers had a molar mass higher than 50 kDa[86,87] which corresponded to oligomers having more than ~11 monomer units. One of the most toxic reported oligomers was identified to be Aβ*56 (56 kDa)[88] corresponding to a dodecamer. Based on the calculations described in this work, a dodecamer would have R_h around 2.8 nm, if it is formed by the superposition of dimers or of monomers (as depicted in [73]). The size of the dodecamer would increase to 3.4 nm if constituted by the superposition of two hexamers. According to another report[10], the toxicity of Aβ(1-42) oligomers decreases with increasing size, and toxic oligomers are likely in the range of 8-24-mers, having an R_h between 3 and 4.2 nm, as calculated in this work. From the CRLI analysis in Figure 5, this fraction of potentially toxic oligomers appears after 30 min, and then tends to decrease in proportion with the aggregation time as the oligomer size is increasing.

Conclusion

This work demonstrates that TDA can be used for the straightforward monitoring of the aggregation of Aβ amyloid peptides. Further, by using an appropriate data treatment of the taylorgrams, one can assess the aggregation pathway by obtaining quantitative data on the proportion and the size of the different aggregated forms. To our knowledge, there is no other real-time aggregation monitoring method reported in the literature allowing to obtain such information in one single analysis. It is worth noting that low volume was used for each aggregation study (total volume of 1µL of a 100 µM peptide solution) with an unprecedented large number of data points during the aggregation process (about 10 points/h) leading to large amount of valuable data.

The results obtained in this work tend to confirm the aggregation pathway of Aβ(1-40) which goes from the monomeric state directly to a fibrillary structure, in contrast to Aβ(1-42) which goes through different intermediate states (oligomers and protofibrils) before reaching the fibrils, in agreement with previous work[58,60]. In addition TDA data gave new insights for the identification of the formed oligomers in the early stages of the aggregation process, including the characterization of the size and abundance evolution of disease-relevant amyloids peptides in solution. The strength of the data processing described in this work lies in its ability to distinguish the small, potentially toxic, oligomers in a polydisperse mixture of larger oligomers, protofibrils and fibrils. In the future, it will be interesting to investigate experimental conditions mimicking the *in vivo* environment, such as lower concentrations of the peptides (in the 100 nM range), mixtures of different amyloid peptides and the physico-chemical properties (ionic strength, pH and composition) mimicking the cerebrospinal fluid.

ACKNOWLEDGEMENTS

LC gratefully acknowledges support from the Institut Universitaire de France (IUF)

Supporting information

Experimental procedure for the synthesis; Theoretical aspects and data processing of TDA; raw TDA data; ThT assay results; DLS results; modelization data.

References

(1) Association, A. s., 2019 Alzheimer's disease facts and figures; Alzheimer's & Dementia 155252602019.

(2) Folch, J.; Ettcheto, M.; Petrov, D.; Abad, S.; Pedrós, I.; Marin, M.; Olloquequi, J.; Camins, A. Review of the advances in treatment for Alzheimer disease: strategies for combating β-amyloid protein. *Neurología (English Edition)* **2018**, *33*, 47-58.

(3) Hardy, J. A.; Higgins, G. A. Alzheimer's disease: the amyloid cascade hypothesis. *Science* **1992**, *256*, 184-185.

(4) Liu, P.-P.; Xie, Y.; Meng, X.-Y.; Kang, J.-S. History and progress of hypotheses and clinical trials for Alzheimer's disease. *Signal Transduction and Targeted Therapy* **2019**, *4*, 29.

(5) Forloni, G.; Balducci, C. Alzheimer's Disease, Oligomers, and Inflammation. *J. Alzheimers Dis.* **2018**, *62*, 1261-1276.

(6) Heppner, F. L.; Ransohoff, R. M.; Becher, B. Immune attack: the role of inflammation in Alzheimer disease. *Nature Reviews Neuroscience* **2015**, *16*, 358-372.

(7) Terry, R. D. The Pathogenesis of Alzheimer Disease: An Alternative to the Amyloid Hypothesis. *J. Neuropathol. Exp. Neurol.* **1996**, *55*, 1023-1025.

(8) Hayden, E. Y.; Teplow, D. B. Amyloid β-protein oligomers and Alzheimer's disease. *Alzheimers Res. Ther.* **2013**, *5*, 60.

(9) Selkoe, D. J.; Hardy, J. The amyloid hypothesis of Alzheimer's disease at 25 years. *EMBO Mol. Med.* **2016**, *8*, 595-608.

(10) Sengupta, U.; Nilson, A. N.; Kayed, R. The Role of Amyloid-β; Oligomers in Toxicity, Propagation, and Immunotherapy. *EBioMedicine* **2016**, *6*, 42-49.

(11) Lambert, M. P.; Barlow, A. K.; Chromy, B. A.; Edwards, C.; Freed, R.; Liosatos, M.; Morgan, T. E.; Rozovsky, I.; Trommer, B.; Viola, K. L.; Wals, P.; Zhang, C.; Finch, C. E.; Krafft, G. A.; Klein, W. L. Diffusible, nonfibrillar ligands derived from $A\beta_{1-42}$ are potent central nervous system neurotoxins. *Proc. Natl. Acad. Sci. U. S. A.* **1998**, *95*, 6448-6453.

(12) Mastroeni, D.; Nolz, J.; Khdour, O. M.; Sekar, S.; Delvaux, E.; Cuyugan, L.; Liang, W. S.; Hecht, S. M.; Coleman, P. D. Oligomeric amyloid β preferentially targets neuronal and not glial mitochondrial-encoded mRNAs. *Alzheimer's & Dementia* **2018**, *14*, 775-786.

(13) Walsh, D. M.; Klyubin, I.; Fadeeva, J. V.; Cullen, W. K.; Anwyl, R.; Wolfe, M. S.; Rowan, M. J.; Selkoe, D. J. Naturally secreted oligomers of amyloid β protein potently inhibit hippocampal long-term potentiation in vivo. *Nature* **2002**, *416*, 535-539.

(14) Salazar, S. V.; Strittmatter, S. M. Cellular prion protein as a receptor for amyloid-β oligomers in Alzheimer's disease. *Biochem. Biophys. Res. Commun.* **2017**, *483*, 1143-1147.

(15) König, A. S.; Rösener, N. S.; Gremer, L.; Tusche, M.; Flender, D.; Reinartz, E.; Hoyer, W.; Neudecker, P.; Willbold, D.; Heise, H. Structural details of amyloid β oligomers in complex with human prion protein as revealed by solid-state MAS NMR spectroscopy. *J. Biol. Chem.* **2021**, 100499.

(16) Guerrero-Muñoz, M. J.; Castillo-Carranza, D. L.; Sengupta, U.; White, M. A.; Kayed, R. Design of Metastable β-Sheet Oligomers from Natively Unstructured Peptide. *ACS Chem. Neurosci.* **2013**, *4*, 1520-1523.

(17) Bemporad, F.; Calloni, G.; Campioni, S.; Plakoutsi, G.; Taddei, N.; Chiti, F. Sequence and structural determinants of amyloid fibril formation. *Acc. Chem. Res.* **2006**, *39*, 620-627.

(18) Ghosh, P.; Kumar, A.; Datta, B.; Rangachari, V. In *BMC Bioinformatics*, 2010, p S24.

(19) Jeong, J. S.; Ansaloni, A.; Mezzenga, R.; Lashuel, H. A.; Dietler, G. Novel mechanistic insight into the molecular basis of amyloid polymorphism and secondary nucleation during amyloid formation. *J. Mol. Biol.* **2013**, *425*, 1765-1781.

(20) Petkova, A. T.; Leapman, R. D.; Guo, Z.; Yau, W. M.; Mattson, M. P.; Tycko, R. Self-propagating, molecular-level polymorphism in Alzheimer's β-amyloid fibrils. *Science* **2005**, *307*, 262-265.

(21) Watanabe-Nakayama, T.; Ono, K.; Itami, M.; Takahashi, R.; Teplow, D. B.; Yamada, M. High-speed atomic force microscopy reveals structural dynamics of amyloid β1-42 aggregates. *Proc. Natl. Acad. Sci. U. S. A.* **2016**, *113*, 5835-5840.

(22) Vassar, P. S.; Culling, C. F. Fluorescent stains, with special reference to amyloid and connective tissues. *Arch. Pathol.* **1959**, *68*, 487-498.

(23) Bieschke, J.; Zhang, Q.; Powers, E. T.; Lerner, R. A.; Kelly, J. W. Oxidative Metabolites Accelerate Alzheimer's Amyloidogenesis by a Two-Step Mechanism, Eliminating the Requirement for Nucleation. *Biochemistry* **2005**, *44*, 4977-4983.

(24) Yang, T.; Li, S.; Xu, H.; Walsh, D. M.; Selkoe, D. J. Large Soluble Oligomers of Amyloid β-Protein from Alzheimer Brain Are Far Less Neuroactive Than the Smaller Oligomers to Which They Dissociate. *The Journal of Neuroscience* **2017**, *37*, 152-163.

(25) Michaels, T. C. T.; Šarić, A.; Curk, S.; Bernfur, K.; Arosio, P.; Meisl, G.; Dear, A. J.; Cohen, S. I. A.; Dobson, C. M.; Vendruscolo, M.; Linse, S.; Knowles, T. P. J. Dynamics of oligomer populations formed during the aggregation of Alzheimer's Aβ42 peptide. *Nat. Chem.* **2020**, *12*, 445-451.

(26) Ono, K.; Condron, M. M.; Teplow, D. B. Structure–neurotoxicity relationships of amyloid β-protein oligomers. *Proc. Natl. Acad. Sci. U. S. A.* **2009**, *106*, 14745.

(27) Zhou, Y.; Liu, J.; Zheng, T.; Tian, Y. Label-Free SERS Strategy for In Situ Monitoring and Real-Time Imaging of Aβ Aggregation Process in Live Neurons and Brain Tissues. *Anal. Chem.* **2020**, *92*, 5910-5920.

(28) Brinet, D.; Kaffy, J.; Oukacine, F.; Glumm, S.; Ongeri, S.; Taverna, M. An improved capillary electrophoresis method for in vitro monitoring of the challenging early steps of Aβ(1-42) peptide oligomerization: Application to anti-Alzheimer's drug discovery. *Electrophoresis* **2014**, *35*, 3302-3309.

(29) Brinet, D.; Gaie-Levrel, F.; Delatour, V.; Kaffy, J.; Ongeri, S.; Taverna, M. In vitro monitoring of amyloid β-peptide oligomerization by Electrospray differential mobility analysis: An alternative tool to evaluate Alzheimer's disease drug candidates. *Talanta* **2017**, *165*, 84-91.

(30) Iuraşcu, M. I.; Cozma, C.; Tomczyk, N.; Rontree, J.; Desor, M.; Drescher, M.; Przybylski, M. Structural characterization of ß-amyloid oligomer-aggregates by ion mobility mass spectrometry and electron spin resonance spectroscopy. *Anal. Bioanal. Chem.* **2009**, *395*, 2509-2519.

(31) Hu, J.; Zheng, Q. Applications of Mass Spectrometry in the Onset of Amyloid Fibril Formation: Focus on the Analysis of Early-Stage Oligomers. *Frontiers in Chemistry* **2020**, *8*, 324.

(32) Bitan, G.; Kirkitadze, M. D.; Lomakin, A.; Vollers, S. S.; Benedek, G. B.; Teplow, D. B. Amyloid β-protein (Aβ) assembly: Aβ40 and Aβ42 oligomerize through distinct pathways. *Proc. Natl. Acad. Sci. U. S. A.* **2003**, *100*, 330-335.

(33) Chamieh, J.; Cottet, H. In *Colloid and Interface Science in Pharmaceutical Research and Development*, Ohshima, H.; Makino, K., Eds.; Elsevier: Amsterdam, 2014, pp 173-192.

(34) Taylor, G. The Dispersion of Matter in Turbulent Flow through a Pipe. *Proc R Soc Lon Ser-A* **1954**, *223*, 446-468.
(35) Taylor, G. Dispersion of Soluble Matter in Solvent Flowing Slowly through a Tube. *Proc R Soc Lon Ser-A* **1953**, *219*, 186-203.
(36) Cottet, H.; Biron, J. P.; Martin, M. Taylor Dispersion Analysis of Mixtures. *Anal. Chem.* **2007**, *79*, 9066-9073.
(37) Bello, M. S.; Rezzonico, R.; Righetti, P. G. Use of Taylor-Aris Dispersion for Measurement of a Solute Diffusion Coefficient in Thin Capillaries. *Science* **1994**, *266*, 773-776.
(38) Sharma, U.; Gleason, N. J.; Carbeck, J. D. Diffusivity of Solutes Measured in Glass Capillaries Using Taylor's Analysis of Dispersion and a Commercial CE Instrument. *Anal. Chem.* **2005**, *77*, 806-813.
(39) Cottet, H.; Martin, M.; Papillaud, A.; Souaïd, E.; Collet, H.; Commeyras, A. Determination of Dendrigraft Poly-l-Lysine Diffusion Coefficients by Taylor Dispersion Analysis. *Biomacromolecules* **2007**, *8*, 3235-3243.
(40) d'Orlyé, F.; Varenne, A.; Gareil, P. Determination of nanoparticle diffusion coefficients by Taylor dispersion analysis using a capillary electrophoresis instrument. *J. Chromatogr. A* **2008**, *1204*, 226-232.
(41) Chamieh, J.; Merdassi, H.; Rossi, J.-C.; Jannin, V.; Demarne, F.; Cottet, H. Size characterization of lipid-based self-emulsifying pharmaceutical excipients during lipolysis using Taylor dispersion analysis with fluorescence detection. *Int. J. Pharm.* **2018**, *537*, 94-101.
(42) Urban, D. A.; Milosevic, A. M.; Bossert, D.; Crippa, F.; Moore, T. L.; Geers, C.; Balog, S.; Rothen-Rutishauser, B.; Petri-Fink, A. Taylor Dispersion of Inorganic Nanoparticles and Comparison to Dynamic Light Scattering and Transmission Electron Microscopy. *Colloid and Interface Science Communications* **2018**, *22*, 29-33.
(43) Pedersen, M. E.; Østergaard, J.; Jensen, H. Flow-Induced Dispersion Analysis (FIDA) for Protein Quantification and Characterization. *Methods Mol. Biol.* **2019**, *1972*, 109-123.
(44) Verpillot, R.; Otto, M.; Klafki, H.; Taverna, M. Simultaneous analysis by capillary electrophoresis of five amyloid peptides as potential biomarkers of Alzheimer's disease. *J. Chromatogr. A* **2008**, *1214*, 157-164.
(45) Botz, A.; Gasparik, V.; Devillers, E.; Hoffmann, A. R. F.; Caillon, L.; Chelain, E.; Lequin, O.; Brigaud, T.; Khemtemourian, L. (R)-α-trifluoromethylalanine containing short peptide in the inhibition of amyloid peptide fibrillation. *Peptide Science* **2015**, *104*, 601-610.
(46) Provencher, S. W. CONTIN: A general purpose constrained regularization program for inverting noisy linear algebraic and integral equations. *Comput. Phys. Commun.* **1982**, *27*, 229-242.
(47) Provencher, S. W. A constrained regularization method for inverting data represented by linear algebraic or integral equations. *Comput. Phys. Commun.* **1982**, *27*, 213-227.
(48) Ortega, A.; Amorós, D.; García de la Torre, J. Prediction of Hydrodynamic and Other Solution Properties of Rigid Proteins from Atomic- and Residue-Level Models. *Biophys. J.* **2011**, *101*, 892-898.
(49) Naiki, H.; Higuchi, K.; Hosokawa, M.; Takeda, T. Fluorometric determination of amyloid fibrils in vitro using the fluorescent dye, thioflavine T. *Anal. Biochem.* **1989**, *177*, 244-249.
(50) Chamieh, J.; Leclercq, L.; Martin, M.; Slaoui, S.; Jensen, H.; Østergaard, J.; Cottet, H. Limits in Size of Taylor Dispersion Analysis: Representation of the Different Hydrodynamic Regimes and Application to the Size-Characterization of Cubosomes. *Anal. Chem.* **2017**, *89*, 13487-13493.

(51) Cottet, H.; Biron, J. P.; Martin, M. On the optimization of operating conditions for Taylor dispersion analysis of mixtures. *Analyst* **2014**, *139*, 3552-3562.

(52) Zheng, J.; Yeung, E. S. Mechanism of Microbial Aggregation during Capillary Electrophoresis. *Anal. Chem.* **2003**, *75*, 818-824.

(53) Schmidt, M.; Sachse, C.; Richter, W.; Xu, C.; Fändrich, M.; Grigorieff, N. Comparison of Alzheimer Aβ(1–40) and Aβ(1–42) amyloid fibrils reveals similar protofilament structures. *Proc. Natl. Acad. Sci. U. S. A.* **2009**, *106*, 19813-19818.

(54) Sachse, C.; Fändrich, M.; Grigorieff, N. Paired β-sheet structure of an Aβ(1-40) amyloid fibril revealed by electron microscopy. *Proc. Natl. Acad. Sci. U. S. A.* **2008**, *105*, 7462-7466.

(55) Yusko, E. C.; Prangkio, P.; Sept, D.; Rollings, R. C.; Li, J.; Mayer, M. Single-Particle Characterization of Aβ Oligomers in Solution. *ACS Nano* **2012**, *6*, 5909-5919.

(56) Cipelletti, L.; Biron, J.-P.; Martin, M.; Cottet, H. Measuring Arbitrary Diffusion Coefficient Distributions of Nano-Objects by Taylor Dispersion Analysis. *Anal. Chem.* **2015**, *87*, 8489-8496.

(57) Arosio, P.; Knowles, T. P. J.; Linse, S. On the lag phase in amyloid fibril formation. *PCCP* **2015**, *17*, 7606-7618.

(58) Chen, Y.-R.; Glabe, C. G. Distinct Early Folding and Aggregation Properties of Alzheimer Amyloid-β Peptides Aβ40 and Aβ42. *J. Biol. Chem.* **2006**, *281*, 24414-24422.

(59) Economou, N. J.; Giammona, M. J.; Do, T. D.; Zheng, X.; Teplow, D. B.; Buratto, S. K.; Bowers, M. T. Amyloid β-Protein Assembly and Alzheimer's Disease: Dodecamers of Aβ42, but Not of Aβ40, Seed Fibril Formation. *J. Am. Chem. Soc.* **2016**, *138*, 1772-1775.

(60) Fu, Z.; Aucoin, D.; Davis, J.; Van Nostrand, W. E.; Smith, S. O. Mechanism of Nucleated Conformational Conversion of Aβ42. *Biochemistry* **2015**, *54*, 4197-4207.

(61) Bitan, G.; Lomakin, A.; Teplow, D. B. Amyloid β-Protein Oligomerization. *J. Biol. Chem.* **2001**, *276*, 35176-35184.

(62) Heyman, H. M.; Zhang, X.; Tang, K.; Baker, E. S.; Metz, T. O. In *Encyclopedia of Spectroscopy and Spectrometry (Third Edition)*, Lindon, J. C.; Tranter, G. E.; Koppenaal, D. W., Eds.; Academic Press: Oxford, 2017, pp 376-384.

(63) Hawe, A.; Hulse, W.; Jiskoot, W.; Forbes, R. Taylor Dispersion Analysis Compared to Dynamic Light Scattering for the Size Analysis of Therapeutic Peptides and Proteins and Their Aggregates. *Pharm. Res.* **2011**, *28*, 2302-2310.

(64) Tomaselli, S.; Esposito, V.; Vangone, P.; van Nuland, N. A. J.; Bonvin, A. M. J. J.; Guerrini, R.; Tancredi, T.; Temussi, P. A.; Picone, D. The α-to-β Conformational Transition of Alzheimer's Aβ-(1–42) Peptide in Aqueous Media is Reversible: A Step by Step Conformational Analysis Suggests the Location of β Conformation Seeding. *Chembiochem* **2006**, *7*, 257-267.

(65) Tran, L.; Basdevant, N.; Prévost, C.; Ha-Duong, T. Structure of ring-shaped Aβ42 oligomers determined by conformational selection. *Sci. Rep.* **2016**, *6*, 21429.

(66) Colvin, M. T.; Silvers, R.; Ni, Q. Z.; Can, T. V.; Sergeyev, I.; Rosay, M.; Donovan, K. J.; Michael, B.; Wall, J.; Linse, S.; Griffin, R. G. Atomic Resolution Structure of Monomorphic Aβ42 Amyloid Fibrils. *J. Am. Chem. Soc.* **2016**, *138*, 9663-9674.

(67) Goddard, T. D.; Huang, C. C.; Meng, E. C.; Pettersen, E. F.; Couch, G. S.; Morris, J. H.; Ferrin, T. E. UCSF ChimeraX: Meeting modern challenges in visualization and analysis. *Protein Sci.* **2018**, *27*, 14-25.

(68) Lührs, T.; Ritter, C.; Adrian, M.; Riek-Loher, D.; Bohrmann, B.; Döbeli, H.; Schubert, D.; Riek, R. 3D structure of Alzheimer's amyloid-β(1–42) fibrils. *Proc. Natl. Acad. Sci. U. S. A.* **2005**, *102*, 17342-17347.

(69) Schmidt, M.; Rohou, A.; Lasker, K.; Yadav, J. K.; Schiene-Fischer, C.; Fändrich, M.; Grigorieff, N. Peptide dimer structure in an Aβ(1–42) fibril visualized with cryo-EM. *Proc. Natl. Acad. Sci. U. S. A.* **2015**, *112*, 11858-11863.

(70) Wälti, M. A.; Ravotti, F.; Arai, H.; Glabe, C. G.; Wall, J. S.; Böckmann, A.; Güntert, P.; Meier, B. H.; Riek, R. Atomic-resolution structure of a disease-relevant Aβ(1–42) amyloid fibril. *Proc. Natl. Acad. Sci. U. S. A.* **2016**, *113*, E4976.

(71) Kreutzer, A. G.; Hamza, I. L.; Spencer, R. K.; Nowick, J. S. X-ray Crystallographic Structures of a Trimer, Dodecamer, and Annular Pore Formed by an Aβ17-36 β-Hairpin. *J. Am. Chem. Soc.* **2016**, *138*, 4634-4642.

(72) Ciudad, S.; Puig, E.; Botzanowski, T.; Meigooni, M.; Arango, A. S.; Do, J.; Mayzel, M.; Bayoumi, M.; Chaignepain, S.; Maglia, G.; Cianferani, S.; Orekhov, V.; Tajkhorshid, E.; Bardiaux, B.; Carulla, N. Aβ(1-42) tetramer and octamer structures reveal edge conductivity pores as a mechanism for membrane damage. *Nature Communications* **2020**, *11*, 3014.

(73) Xiao, Y.; Ma, B.; McElheny, D.; Parthasarathy, S.; Long, F.; Hoshi, M.; Nussinov, R.; Ishii, Y. Aβ(1–42) fibril structure illuminates self-recognition and replication of amyloid in Alzheimer's disease. *Nat. Struct. Mol. Biol.* **2015**, *22*, 499-505.

(74) Cohen, S. I. A.; Linse, S.; Luheshi, L. M.; Hellstrand, E.; White, D. A.; Rajah, L.; Otzen, D. E.; Vendruscolo, M.; Dobson, C. M.; Knowles, T. P. J. Proliferation of amyloid-β42 aggregates occurs through a secondary nucleation mechanism. *Proc. Natl. Acad. Sci. U. S. A.* **2013**, *110*, 9758-9763.

(75) Cohen, S. I. A.; Vendruscolo, M.; Welland, M. E.; Dobson, C. M.; Terentjev, E. M.; Knowles, T. P. J. Nucleated polymerization with secondary pathways. I. Time evolution of the principal moments. *J. Chem. Phys.* **2011**, *135*, 065105.

(76) Knowles, T. P. J.; Waudby, C. A.; Devlin, G. L.; Cohen, S. I. A.; Aguzzi, A.; Vendruscolo, M.; Terentjev, E. M.; Welland, M. E.; Dobson, C. M. An Analytical Solution to the Kinetics of Breakable Filament Assembly. *Science* **2009**, *326*, 1533-1537.

(77) Lee, C.-T.; Terentjev, E. M. Mechanisms and rates of nucleation of amyloid fibrils. *J. Chem. Phys.* **2017**, *147*, 105103.

(78) Srivastava, A. K.; Pittman, J. M.; Zerweck, J.; Venkata, B. S.; Moore, P. C.; Sachleben, J. R.; Meredith, S. C. β-Amyloid aggregation and heterogeneous nucleation. *Protein Sci.* **2019**, *28*, 1567-1581.

(79) Shea, D.; Hsu, C.-C.; Bi, T. M.; Paranjapye, N.; Childers, M. C.; Cochran, J.; Tomberlin, C. P.; Wang, L.; Paris, D.; Zonderman, J.; Varani, G.; Link, C. D.; Mullan, M.; Daggett, V. α-Sheet secondary structure in amyloid β-peptide drives aggregation and toxicity in Alzheimer's disease. *Proc. Natl. Acad. Sci. U. S. A.* **2019**, *116*, 8895-8900.

(80) Ahmed, M.; Davis, J.; Aucoin, D.; Sato, T.; Ahuja, S.; Aimoto, S.; Elliott, J. I.; Van Nostrand, W. E.; Smith, S. O. Structural conversion of neurotoxic amyloid-β1–42 oligomers to fibrils. *Nat. Struct. Mol. Biol.* **2010**, *17*, 561-567.

(81) Ghosh, P.; Vaidya, A.; Kumar, A.; Rangachari, V. Determination of critical nucleation number for a single nucleation amyloid-β aggregation model. *Math. Biosci.* **2016**, *273*, 70-79.

(82) Gremer, L.; Schölzel, D.; Schenk, C.; Reinartz, E.; Labahn, J.; Ravelli, R. B. G.; Tusche, M.; Lopez-Iglesias, C.; Hoyer, W.; Heise, H.; Willbold, D.; Schröder, G. F. Fibril structure of amyloid-β(1-42) by cryo-electron microscopy. *Science* **2017**, *358*, 116-119.

(83) Novo, M.; Freire, S.; Al-Soufi, W. Critical aggregation concentration for the formation of early Amyloid-β (1–42) oligomers. *Sci. Rep.* **2018**, *8*, 1783.

(84) Mastrangelo, I. A.; Ahmed, M.; Sato, T.; Liu, W.; Wang, C.; Hough, P.; Smith, S. O. High-resolution Atomic Force Microscopy of Soluble Aβ42 Oligomers. *J. Mol. Biol.* **2006**, *358*, 106-119.

(85) Nirmalraj, P. N.; List, J.; Battacharya, S.; Howe, G.; Xu, L.; Thompson, D.; Mayer, M. Complete aggregation pathway of amyloid beta (1-40) and (1-42) resolved on an atomically clean interface. *Sci Adv* **2020**, *6*, eaaz6014.

(86) Lacor, P. N.; Buniel, M. C.; Furlow, P. W.; Sanz Clemente, A.; Velasco, P. T.; Wood, M.; Viola, K. L.; Klein, W. L. Aβ Oligomer-Induced Aberrations in Synapse Composition, Shape, and Density Provide a Molecular Basis for Loss of Connectivity in Alzheimer's Disease. *The Journal of Neuroscience* **2007**, *27*, 796.

(87) Velasco, P. T.; Heffern, M. C.; Sebollela, A.; Popova, I. A.; Lacor, P. N.; Lee, K. B.; Sun, X.; Tiano, B. N.; Viola, K. L.; Eckermann, A. L.; Meade, T. J.; Klein, W. L. Synapse-Binding Subpopulations of Aβ Oligomers Sensitive to Peptide Assembly Blockers and scFv Antibodies. *ACS Chem. Neurosci.* **2012**, *3*, 972-981.

(88) Lesné, S.; Koh, M. T.; Kotilinek, L.; Kayed, R.; Glabe, C. G.; Yang, A.; Gallagher, M.; Ashe, K. H. A specific amyloid-β protein assembly in the brain impairs memory. *Nature* **2006**, *440*, 352-357.

for Table of Contents only